INSTITUTE OF PHYSICS PUBLISHING MODELLING AND SIMULATION IN MATERIALS SCIENCE AND ENGINEERING

Modelling Simul. Mater. Sci. Eng. **11** (2003) 553–574 PII: S0965-0393(03)63246-8

Modelling of semi-solid processing using a modified temperature-dependent power-law model

L Orgéas[1,3,4], J-P Gabathuler[2], Th Imwinkelried[2], Ch Paradies[1,5] and M Rappaz[1]

[1] Laboratoire de Métallurgie Physique, Ecole Polytechnique Fédérale de Lausanne MX-G, CH-1015 Lausanne, Switzerland
[2] Alusuisse T & M Ltd, Technology Center, Badische Bahnhofstrasse 16, CH-8212 Neuhausen-am-Rheinfall, Switzerland

E-mail: Laurent.Orgeas@hmg.inpg.fr

Received 15 January 2003, in final form 4 May 2003
Published 13 June 2003
Online at stacks.iop.org/MSMSE/11/553

Abstract

A fairly simple one-phase rheological model has been implemented into a commercial fluid flow finite element software to simulate mould filling during the semi-solid processing (thixoforming) of aluminium alloys. This model is of purely viscous nature. Its temperature-dependent viscosity is a power-law function of the shear rate with a shear rate cut-off. The constitutive parameters of this model were determined for a rheocast A356 alloy. For that purpose, simulation results were compared with instrumented thixoforming experiments performed on a production-scale injection machine. The selected configuration was that of a transient flow near a bifurcation, i.e. obstruction of an established Poiseuille-type flow by a shaft placed at the centre of a tube. Using these parameters, the model was then further validated by comparing the simulation of an axisymmetric reservoir mould filling with the shape of solidified shells obtained after interrupted injection experiments.

1. Introduction

In order to produce high security and near net-shape metal components with reduced porosity and shrinkage, processing of metals in the semi-solid state is viewed as an attractive and promising manufacturing method. Among several advantages, the increased viscosity of semi-solid alloys makes the flow much more laminar during the injection stage, thus reducing the entrapment of oxide skins. However, the complex shear-thinning behaviour of metallic alloys

[3] Author to whom correspondence should be addressed.
[4] Present address: Laboratoire Sols—Solides—Structures, CNRS—Institut National Polytechnique de Grenoble—Université Joseph Fourier, BP. 53, 38 041 Grenoble Cedex 9, France.
[5] Present address: Ostrolenk, Faber, Gerb & Soffen LLP, 1180 av. of the Americas, NY 10036-8403, USA.

is also associated with flow instabilities and segregation during the non-uniform loading of an injection process such as thixoforming. Therefore, the optimization of semi-solid metal (SSM) processes requires many trials whenever a new design has to be produced. Accurate simulation of thixoforming could possibly reduce the number of casting trials required prior to determining the optimal process parameters for a given component. However, numerical simulation requires a fairly accurate knowledge of both the boundary conditions and SSM rheological behaviour. As for many casting or forging processes, mechanical and thermal boundary conditions between the mould and the material are extremely complex and interdependent during thixoforming [1]. On the other hand, the time-, strain rate- and temperature-dependent rheological behaviour [2–4] of SSM has been rarely measured under the very high strain-rates encountered in industrial conditions. Segregation between the solid and liquid phases also encountered in industrial conditions [5–7], induced either during the non-uniform mechanical loading of the billet or near the highly sheared periphery zone of a SSM flow, is a further complication in a consistent modelling approach.

In this work, the modelling of the thixoforming process of a rheocast aluminium A356 alloy has been attempted under conditions close to industrial production. In a first step, the bifurcation of a Poiseuille-type flow near a shaft inserted inside a tube is investigated during instrumented thixocasting experiments (section 2). A fairly simple phenomenological model suitable to reproduce the rheological behaviour of the SSM under such conditions is proposed and implemented in the commercial finite element software ProCAST^{TM}. This model, which is based on a modified one-phase power-law model with a shear cut-off (PLCO), is described in section 3. By comparing the simulation results with the shaft experiments, the parameters of the PLCO model are determined (see section 4). The model is then further validated by comparing the calculated flow during filling of a reservoir with the solidified shells obtained after interrupted injection experiments (section 5). Finally, this modelling methodology is discussed and analysed in section 6.

2. Experiments

The alloy used for the experiments was an Al—7 wtpct Si—0.3 wtpct Mg alloy (A356) produced semi-continuously by rheocasting by Alusuisse [8]. Its initial microstructure was made of fairly homogeneous fine spheroidal Al grains surrounded by a fine eutectic phase. The 75 mm diameter billets of this alloy were then cut and heated up to a given initial volume fraction of solid $f_{s,ini}$ by inductive heating. The SSM billet was then inserted into the shot-sleeve of a Bühler industrial shot-controlled pressure die casting machine (inner diameter of the shot-sleeve ϕ_{ram}: 78 mm). Two series of experiments, which are described in the following subsections, were carried out for the determination of the rheological behaviour of the A356 alloy in the semi-solid state [1].

2.1. Axisymmetric Poiseuille-type experiments

In these first tests, the axisymmetric horizontal mould was simply made of a 350 mm long tube of constant diameter, ϕ_{tube}, connected to an axisymmetric reservoir at the end (see figure 1(*a*)). During the experiments, the pressure and temperature were measured at different positions by sensors and thermocouples. After filling the entire tube, the piston was abruptly stopped in a position such that the end reservoir was only partially filled. The shape of the material that had solidified at the surface of the reservoir material was then analysed. The main parameters which were varied in these experiments were the initial volume fraction of solid $f_{s,ini}$ ($\approx$0.73, 0.58 and 0.52), the diameter of the long tube ϕ_{tube} (=10, 20, 25, and 40 mm), and the velocity

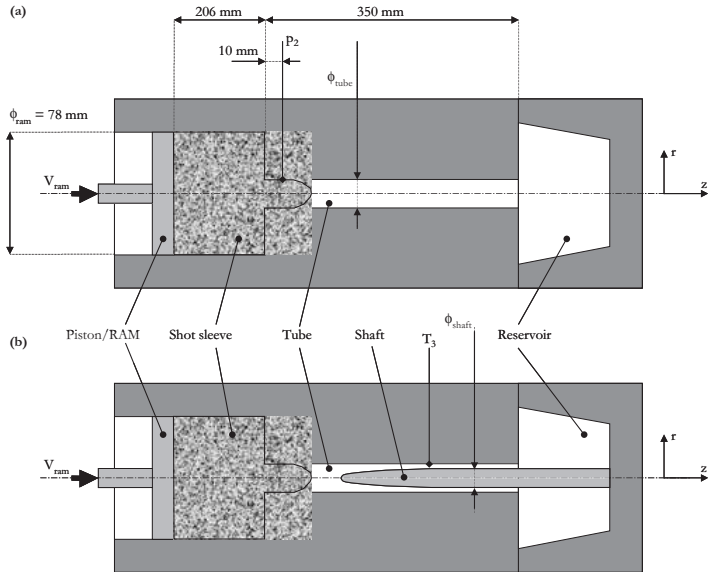

Figure 1. Experimental set-up used for the Poiseuille-type flow (*a*) and for the bifurcation of a Poiseuille-type flow near the parabolic tip of an axisymmetric shaft ('shaft experiment') (*b*).

of the injection piston $v_{\mathrm{ram}}(t)$ whose normalized time-evolution is shown in figure 2(*a*): after an initial and rapid transient from 0 to a given value $v_{\mathrm{ram},0}$, $v_{\mathrm{ram}}(t)$ was maintained constant and was rapidly decreased at the end of the test to zero. $v_{\mathrm{ram},0}$ was varied between 0.2 and $0.8\,\mathrm{m\,s^{-1}}$. Two important results were underlined with these tests.

(i) The recorded pressure p_2 (see figure 1) was extremely low, as a matter of fact below the sensitivity of the pressure sensor which was of the order of 0.1 bar (figure 2(*a*)). This value is much lower than what could be expected from a standard no-slip Poiseuille flow analysis using a power-law fluid [1] and an averaged value of typically 10 Pa s reported in the literature for the viscosity of SSM under such conditions [3]. As shown by the cross-section of the SSM remaining in the long tube after the test (figure 2(*b*)), it was found that this discrepancy could be explained by the presence of a thin segregated liquid layer of nearly eutectic composition (eutectic layer (EL)) near the surface of the tube wall. Such a local segregation phenomenon has already been observed in particulate suspensions similar to semi-solid slurry [9]. As a consequence, the SSM in the tube behaved like a solid plug ('plug flow'), almost all of the shear rate being accommodated by this thin layer of liquid (i.e. replacement of the no-slip condition by a free-slip one). This was confirmed by the observation of the free surface of the metal when the injection experiment was interrupted with the long tube only partially filled: the end of the SSM rod was almost like a tooth-paste extruded out of a thin EL solidified skin.

(ii) When the experiments were interrupted while the SSM already filled partially the reservoir, it was found that the shape of the cast alloy that had solidified at the surface of the reservoir was a function of both the initial volume fraction of solid $f_{\mathrm{s,ini}}$ and the imposed process parameters ϕ_{tube} and v_{ram}. Different shapes such as 'disk + shell', 'disk' and 'mound' fillings, were observed [10]. These filling morphologies will be used in section 4 of this paper for the validation of the rheological model used in this work and described in section 3.

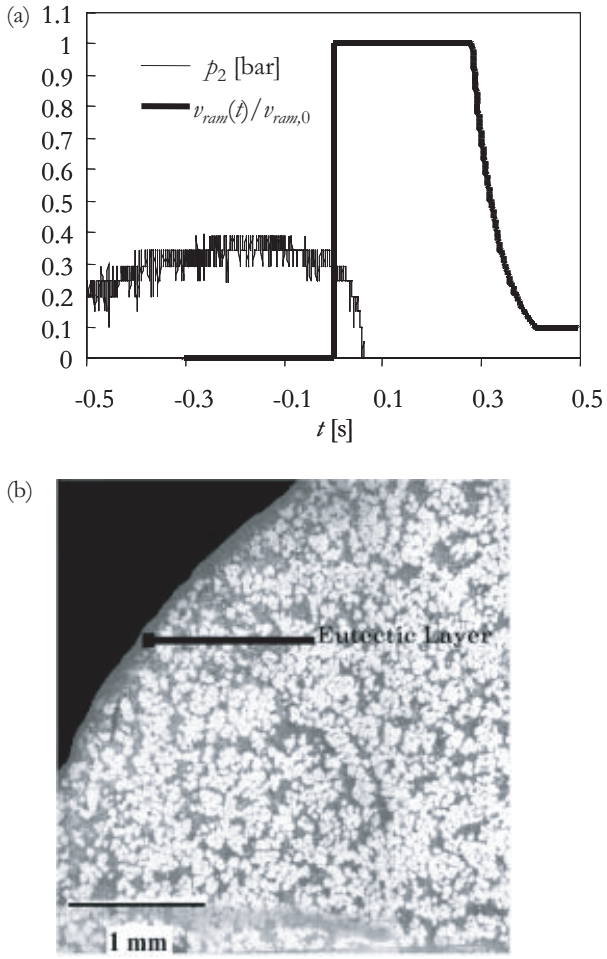

Figure 2. (*a*) Time-evolutions of the pressure p_2 and of the normalized piston velocity $v_{\mathrm{ram}}(t)/v_{\mathrm{ram},0}$ in the Poiseuille-type experiment (figure 1(*a*)) performed with $f_{\mathrm{s,ini}} = 0.73$, $\phi_{\mathrm{tube}} = 25\,\mathrm{mm}$ and $v_{\mathrm{ram},0} = 0.8\,\mathrm{m\,s^{-1}}$. (*b*) Corresponding cross-section of the SSM cylinder solidified in the tube showing the segregation of a thin eutectic liquid layer (EL) near the surface of the tube.

2.2. Bifurcation of a Poiseuille-type flow near a shaft ('shaft experiment')

The experimental set-up shown in figure 1(*a*) was modified in order to study the bifurcation of a Poiseuille-type flow in the long tube near an obstacle. For that purpose, a parabolic-tip shaft was fixed to the back of the reservoir so that it entered the tube in an axisymmetric configuration, as shown in figure 1(*b*). The shaft, whose diameter ϕ_{shaft} was 18 mm, was inserted in the 25 mm diameter tube over a length of approximately 150 mm.

As can be seen in figure 3, the results of these 'shaft' experiments are quite different from those obtained under steady-state Poiseuille-type conditions. First, as shown in figure 3(*a*), the pressure p_2 (see figure 1(*b*)) raised to a maximum of about 350 bar, i.e. a value which is two to three orders of magnitude larger than the pressures measured in the set-up of figure 1(*a*). The time-evolution of the pressure systematically showed two stages: a first and rapid increase up to a maximum or peak value, p_{peak}, quickly followed by a rapid decrease

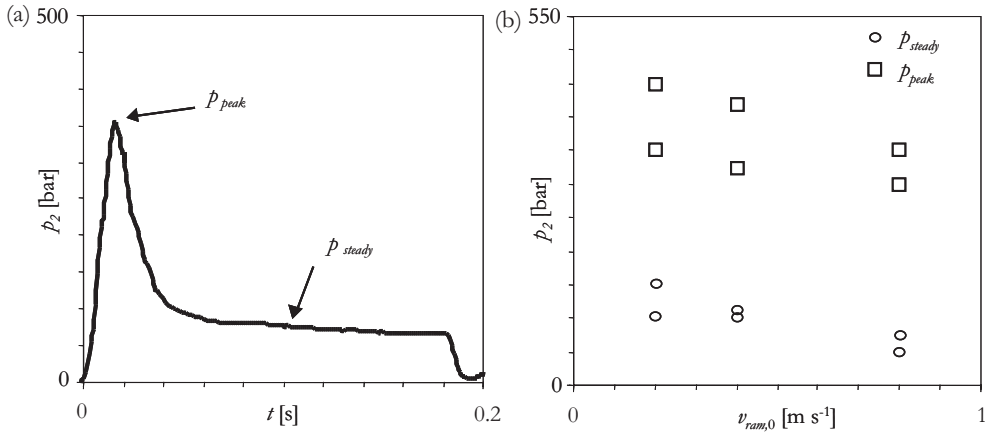

Figure 3. Time-evolution of the pressure, p_2, measured during the shaft experiment performed at $v_{\mathrm{ram},0} = 0.8\,\mathrm{m\,s^{-1}}$ (*a*); maximum pressure, p_{peak}, and pressure measured in the nearly steady-state regime, p_{steady}, as a function of the piston ram velocity, $v_{\mathrm{ram},0}$ (*b*). Other conditions are: $f_{\mathrm{s,ini}} = 0.58$, $\phi_{\mathrm{tube}} = 25\,\mathrm{mm}$ and $\phi_{\mathrm{shaft}} = 18\,\mathrm{mm}$.

to a 'steady-state' pressure, p_{steady} (the final pressure drop near 0.2 s in figure 3(*a*) corresponds to the end of the injection process). As illustrated in figure 3(*b*), both the peak and steady-state pressures are decreasing functions of the velocity of the piston $v_{\mathrm{ram},0}$. For each of the three velocities investigated here (0.2, 0.4 and $0.8\,\mathrm{m\,s^{-1}}$), two sets of experiments were performed: the scattering of the points (as much as 50% difference for the same experimental conditions) illustrates the uncertainty of these *in situ* tests. Nevertheless, the decrease of p_2 with an increasing $v_{\mathrm{ram},0}$ is surprising, even for a shear-thinning material: when the shear rate (and thus piston velocity) is increased, the viscosity decreases but the stress level (and thus measured pressure) should increase. It will be shown that the opposite trend seen in figure 3(*b*) is due to thermal effects which affect the volume fraction of solid of the SSM and thus its viscosity, this effect dominating in this situation is associated with a shear rate variation.

3. Theoretical and numerical background

Modelling and simulation of SSM processing have been achieved with essentially two different approaches: two-phase [11–17] and one-phase approaches [18–22]. In the first category, the SSM is considered as a saturated two-phase medium, i.e. made of the liquid and solid phases. Each phase has its own behaviour, which can be influenced by the presence of the other phase via interfacial contributions. The conservation equations can be written within a mixture theory background [23] and the solid phase (solid skeleton) can be modelled as a purely viscous and compressive medium [11, 13]. Momentum exchanges between the solid and the Newtonian liquid are handled by a Darcy-type term appearing in momentum equations [24]. These models are very attractive because they are able to predict phase separation arising during thixoforming [12, 16, 17]. However, the determination of the associated rheological constitutive parameters they require is not straightforward: intensive experimental studies achieved on specific rheometers are often needed (e.g. drained tests for the study of the rheology of the solid skeleton, [11, 13]). Moreover, two-phase models usually require the simultaneous calculation of a solid fraction field, a pressure field, two velocity fields (for the liquid and the solid), and a temperature field (in most cases isothermal simulation is performed), so that the

simulation needs very high computation time. For these reasons, such models have never been used in three-dimensional industrial simulation software yet, to the best of our knowledge.

In the second approach, the SSM is supposed to behave like a homogeneous medium in which the solid and liquid phases move at the same velocity. Although such a strong assumption limits the validity domain of one-phase models and does not allow to account for phase separation, some of these one-phase models can be sophisticated. Using internal variables [25], they can simulate thixotropic effects induced by structural evolutions of the solid phase such as agglomeration and disagglomeration phenomena.

The PLCO model that has been developed and used in this work belongs to this second category. Although simpler than the model of Kumar *et al* [18], it has the advantage that it can be applied to a wider solidification interval, i.e. from $f_s = 0$ to 1, at least theoretically. The major assumption of the PLCO model are that the material is seen as a purely viscous isotropic and incompressible fluid.

In order to perform the mould filling simulation of SSM industrial parts, this model has been implemented in the commercial finite element code ProCAST^{TM}. Within the framework of a Eulerian description, this software is capable of solving simultaneously three-dimensional transient thermal and fluid flow problems with free surfaces. The set of partial differential equations to be solved is briefly summarized below:

- Mass balance:

$$\frac{\partial}{\partial t}\rho + \operatorname{div}(\rho \underline{v}) = 0 \tag{1}$$

  where ρ and $\underline{v}$ are the volumetric mass and the velocity of the fluid, respectively.
- Momentum balance:

$$\frac{\partial}{\partial t}(\rho \underline{v}) + \underline{\mathbf{div}}(\rho \underline{v} \otimes \underline{v}) = -\underline{\mathbf{grad}}\, p + \underline{\mathbf{div}}\, \underline{\underline{\sigma}}^{v} + \rho \underline{g} \tag{2}$$

  where $\underline{g}$ is the gravitation vector, p the fluid pressure, and $\underline{\underline{\sigma}}^{v}$ the viscous stress tensor.
- Energy balance, written as an enthalpy formulation:

$$\frac{\partial}{\partial t}(\rho h) + \operatorname{div}(\rho h \underline{v}) = \operatorname{div}(\kappa\, \underline{\mathbf{grad}}\, T) + Q_{\text{mech}} \tag{3}$$

  In this equation, Q_{mech} is a volumetric heat source that accounts for mechanically induced dissipation effects, T is the temperature, κ is the thermal conductivity of the medium and h its specific enthalpy. Please note that the entire enthalpy is transported with the velocity of the fluid, i.e. that the solid and liquid phases composing the SSM have the same velocity. In order to account for solidification, ρh is written as follows:

$$\rho h = \int_0^T \rho c_p(\theta)\, \mathrm{d}\theta + \rho L(1 - f_s) \tag{4}$$

  where c_p and L are the specific heat and latent heat of fusion, respectively, and f_s is the volume fraction of solid of the SSM.
- Free surface modelling, achieved with a scalar variable, Φ, describing the local volume fraction of the SSM fluid (i.e. $\Phi = \frac{0}{1}$ if the 'point' is empty/full of SSM). Previous balance equations are averaged with this variable, which is advected according to:

$$\frac{\partial}{\partial t}\Phi + \underline{v} \cdot \underline{\mathbf{grad}}\, \Phi = 0 \tag{5}$$

The three-dimensional rheological behaviour of the SSM is described using a simple tensorial relationship between the viscous stress tensor, $\underline{\underline{\boldsymbol{\sigma}}}^v$, and the strain rate tensor, $\underline{\underline{\boldsymbol{D}}}$:

$$\underline{\underline{\boldsymbol{\sigma}}}^v = 2\mu\underline{\underline{\boldsymbol{D}}} \qquad \text{where } \underline{\underline{\boldsymbol{D}}} = \tfrac{1}{2}(\underline{\underline{\mathbf{grad}}}\,\underline{\boldsymbol{v}} + {}^{\mathrm{T}}\underline{\underline{\mathbf{grad}}}\,\underline{\boldsymbol{v}}) \tag{6}$$

where μ is the semi-solid viscosity. In this work, μ is a function of the equivalent shear rate $\dot{\gamma}$:

$$\dot{\gamma} = \sqrt{2\underline{\underline{\boldsymbol{D}}} : \underline{\underline{\boldsymbol{D}}}} \tag{7}$$

In order to account for the shear-thinning behaviour of SSM, the PLCO model supposes a modified power-law relationship between μ and $\dot{\gamma}$:

$$\mu = \mu_0 \left(\frac{\dot{\gamma}}{\dot{\gamma}_{\mathrm{c}}}\right)^{n-1} \qquad \text{if } \dot{\gamma} \geqslant \dot{\gamma}_0 \tag{8a}$$

$$\mu = \mu_0 \left(\frac{\dot{\gamma}_0}{\dot{\gamma}_{\mathrm{c}}}\right)^{n-1} \qquad \text{if } \dot{\gamma} < \dot{\gamma}_0 \tag{8b}$$

where μ_0 is the temperature-dependent semi-solid viscosity defined at a characteristic shear strain rate $\dot{\gamma}_{\mathrm{c}}$ (set to $1\ \mathrm{s}^{-1}$ in this work), n is the shear-rate sensitivity coefficient and $\dot{\gamma}_0$ is the shear rate cut-off. The shear rate cut-off $\dot{\gamma}_0$ was initially used in finite element codes to improve numerical convergence for shear-thinning materials ($n < 1$) when the shear rate decreased toward zero. Another point of view is adopted in this work. The thixotropic behaviour of SSM is strongly related to the structural evolutions occurring during deformation, namely agglomeration, disagglomeration, round-off of solid particles, etc [3]:

- Agglomeration and coalescence of grains probably does not take place over the very short injection times characteristics of thixoforming [3, 15]. Therefore, a decrease of $\dot{\gamma}$ is most likely not to modify (increase) the viscosity μ of the SSM.
- On the contrary, disagglomeration and round-off of particles occur over timescales much shorter and a sudden increase of the shear rate, $\dot{\gamma}$, will most likely decrease the viscosity μ of the semi-solid suspension.

In other words, an increase of $\dot{\gamma}$ beyond the largest shear rate, $\dot{\gamma}_0$, experienced so far by the SSM decreases its viscosity (and of course modifies the value of the maximum shear rate $\dot{\gamma}_0$). On the contrary, a decrease of $\dot{\gamma}$ below the actual value, $\dot{\gamma}_0$, will not modify the viscosity (and leaves $\dot{\gamma}_0$ unchanged), at least during the injection of the billet. This 'ratchet-type' behaviour of the viscosity of SSM could be modelled accurately. However, in the experiments presented in section 2, as the main evolution of the grain structure and associated viscosity is observed in the transition between the shot-sleeve and the small injection aperture (or long tube, see figure 1), only one value of $\dot{\gamma}_0$ (i.e. the maximum on the axis location) in this high shear rate region has been used in this simulation. If $\dot{\gamma} > \dot{\gamma}_0$, the SSM becomes more fluid, whereas if $\dot{\gamma} < \dot{\gamma}_0$, its viscosity resumes to the value it had at the exit of the shot-sleeve.

As stated before, the viscosity is also strongly dependent on the volume fraction of solid, and hence on the temperature of the billet [2]. To account for such a dependency, the viscosity μ_0 and the shear rate sensitivity n, were made f_{s}-dependent through the empirical relationships:

$$\mu_0 = \mu_{\mathrm{liquid}} \exp(B f_{\mathrm{s}}) \tag{9a}$$

$$n = \frac{1 - n_{\min}}{2}\left[1 - \tanh\left(\frac{2\alpha(f_{\mathrm{s}} - f_{\mathrm{s},0})}{1 - n_{\min}}\right)\right] + n_{\min} \tag{9b}$$

The phenomenological relation (9a) has been proposed by other authors to estimate μ_0 [5, 26, 27]. Given volume fraction of solid, it involves two parameters: μ_{liquid}, the Newtonian

viscosity of the pure liquid phase, and B, a parameter that mainly depends on the microstructure of the SSM. Equation (9*b*) is proposed in this work on the basis of two asymptotic limits. At high volume fractions of solid, the SSM shear rate sensitivity n should tend to the value $n_{\min}$ characteristics of the creep behaviour of the solid phase ($\sim$0.2–0.25), whereas, at low f_s, the SSM behaviour should be that of a Newtonian liquid (i.e. $n = 1$). The transition between these two well-known deformation modes is achieved at a 'critical' value of the solid fraction, $f_{s,0}$, with a 'slope' dn/df_s equal to α.

Finally, the PLCO model being a purely viscous fluid model, the volumetric heat source term Q_{mech} becomes:

$$Q_{\text{mech}} = \underline{\underline{\boldsymbol{\sigma}}}^{v} : \underline{\underline{\boldsymbol{D}}} = 2\mu \underline{\underline{\boldsymbol{D}}} : \underline{\underline{\boldsymbol{D}}} \tag{10}$$

In ProCAST^{TM}, the subsets of equations {(1), (2), (6), (7), (8), (9)}, {(3), (4), (10)} and {(5)}, whose nodal unknowns are, respectively, ($\underline{\boldsymbol{v}}$, p), (h, T) and ($\boldsymbol{\Phi}$), are solved successively [28]. A streamline upwinding (SU) method is used to compute all the advection terms appearing in these equations. A Newton–Raphson scheme is employed to solve non-linear subsets of equations {(1), (2), (6), (7), (8), (9)} and {(3), (4), (10)}. A segmented solution algorithm, similar to the SIMPLE algorithm, allows the calculation of $\underline{\boldsymbol{v}}$ and p. At last, the free surface motion algorithm used to solve (5) is a continuum advection scheme [28].

In summary, the PLCO model requires the knowledge of few constitutive parameters: the shear rate cut-off $\dot{\gamma}_0$, which is mainly dependent on the geometry of the considered problem, the viscosity of the liquid phase μ_{liquid}, and the parameter B, both used to define the viscosity μ_0 as a function of f_s (cf equation (9*a*)), and the three parameters $n_{\min}$, α and $f_{s,0}$, that give the evolution of the shear rate sensitivity n (cf equation (9*b*)). The following section gives the methodology adopted to determine these parameters.

4. Modelling

In order to reproduce the behaviour of the rheocast A356 alloy during the injection of SSM, different steps were performed. First, assumptions were made on the material properties. Second, two rheological parameters were determined using both the simulation and the experiments presented in section 2. Unless otherwise specified, the common numerical assumptions for the results presented below were: no gravity effects, axisymmetric thermo-mechanical calculations, rheological behaviour of the material given by the temperature-dependent PLCO model and free-slip boundary conditions between the mould and the SSM (see figure 2(*b*)).

4.1. Material properties

The values of the material parameters given in this section correspond to those of the Al—7 wtpct Si—0.3 wtpct Mg (A356) alloy used in the experiments. The evolution of the volume fraction of solid f_s as a function of the temperature was determined by thermal analysis and is illustrated in figure 4(*a*). In this figure, the three initial solid fractions $f_{s,\text{ini}}$, that were used in the experiments are also indicated by small dots. The other thermo physical properties of this alloy are given in table 1. Using the specific heat c_p, the specific latent heat l, and the f_s evolution plotted in figure 4(*a*), the volumetric enthalpy ρh was calculated according to equation (4).

To run the simulation some assumptions were made on the constitutive parameters of the PLCO model. First, the shear-rate sensitivity n was supposed to obey to equation (9*b*). Based on the experimental results obtained for the same alloy by Nguyen [29], $n_{\min}$, $f_{s,0}$ and α were

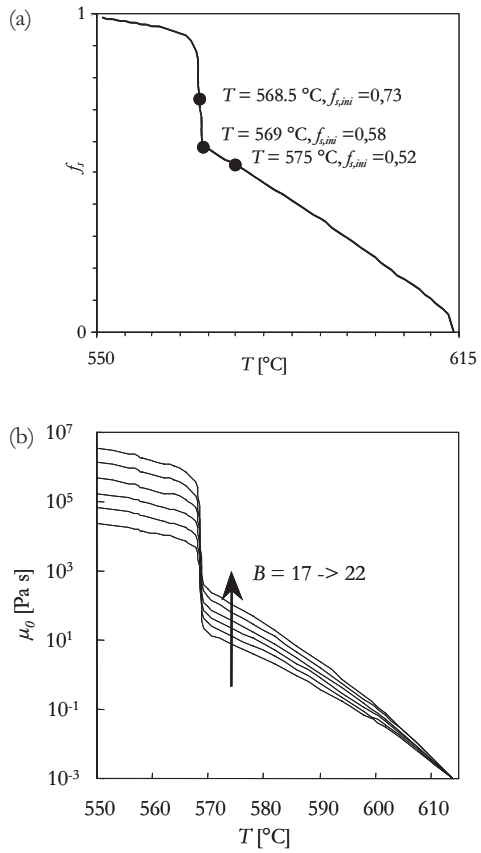

Figure 4. (*a*) Evolution of the volume fraction of solid, f_s, as a function of the temperature, T, as measured by thermal analysis for the A356 alloy. The small dots indicate the three initial solid fractions, $f_{s,ini}$, used in the injection experiments. (*b*) Temperature-dependence of the viscosity, μ_0, for five values of B ranging from 17 to 22.

Table 1. Thermo physical and rheological properties of the A356 alloy.

Specific mass, ρ	$T = 560^{\circ}$C	2580	$\mathrm{kg\,m^{-3}}$
	$T = 615^{\circ}$C	2380	
Specific latent heat of fusion, L		389 000	$\mathrm{J\,kg^{-1}}$
Specific heat, c_p		900	$\mathrm{J\,kg^{-1}\,K^{-1}}$
Thermal conductivity, κ		150	$\mathrm{W\,m^{-1}\,K^{-1}}$
Dynamic viscosity of liquid Al, μ_{liquid}		1×10^{-3}	Pa s
Minimum strain-rate sensitivity, n_{min}		0.25	—
Critical fraction of solid, $f_{\mathrm{s},0}$		0.35	—
Parameter, α		2.5	—
Parameter, B		22	—
Parameter, β		2.34	—
Parameter, χ		2.14	—

fixed to 0.25, 0.35 and 2.5, respectively, as illustrated in figure 5. Second, the viscosity μ_{liquid} of molten aluminium (equation (9*a*)) was fixed to a standard value of 10^{-3} Pa s. Finally, to estimate the evolution of the consistency μ_0 as a function of f_s or T, different values of B were tested, ranging from 15 to 25. These high values correspond to the experimental results

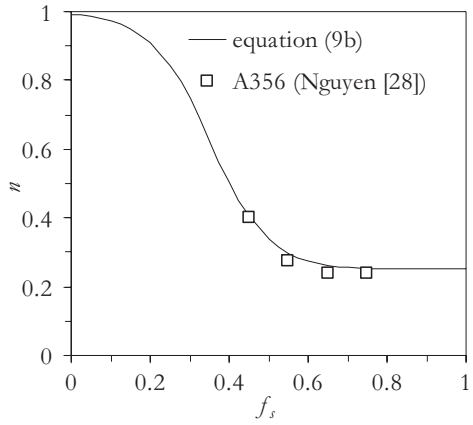

Figure 5. Evolution of the shear-rate sensitivity n as a function of the solid volume fraction f_s for the A356 alloy—comparison between data obtained by Nguyen [28] and the fit of equation (9*b*) with $n_{min} = 0.25$, $f_{s,0} = 0.35$ and $\alpha = 2.5$.

given in the literature for SSM [5, 26]. As examples, the evolution of μ_0 as a function of T is plotted in figure 4(*b*) when B ranges from 17 to 22: all the curves start at μ_{liquid} at the liquidus temperature (i.e. for $f_s = 0$). Regardless of the value selected for B, very large variations of μ_0 are expected, especially during eutectic solidification.

4.2. Determination of the cut-off value

As explained in section 3, the shear rate cut-off $\dot{\gamma}_0$ was used to account for structural evolution occurring in high shear-rate regions and to subsequently limit the minimum viscosity of the SSM to the value it had reached in such regions. According to figure 1, it is reasonable to assume that one obvious high shear-rate region is located between the shot-sleeve and the entrance of the narrow tube. Using a simple mass balance argument, the mean velocity of the SSM in the tube, v_{tube}, is simply given by: $v_{\text{tube}} = (\phi_{\text{shotsleave}}/\phi_{\text{tube}})^2 v_{\text{ram}}$. From that, it is possible to get a first rough estimation of the shear rate value $\dot{\gamma}_0$ occurring in such a region. Assuming that $\phi_{\text{shotsleave}} \gg \phi_{\text{tube}}$ and that the velocity gradient of the SSM is located in a region $\Delta z \approx \phi_{\text{tube}}$ ahead of the entrance of the tube, the horizontal component of the velocity field gradient gives:

$$\dot{\gamma}_0 \approx \dot{\gamma}_{zz} \approx 2\frac{\Delta v_z}{\Delta z} = 2\left[\left(\frac{\phi_{\text{shotsleave}}}{\phi_{\text{tube}}}\right)^2 - 1\right] \approx 2\left(\frac{\phi_{\text{shotsleave}}}{\phi_{\text{tube}}}\right)^2 \frac{v_{\text{ram}}}{\phi_{\text{tube}}} \tag{11}$$

As a result of the mass balance, the maximum shear rate in this region $\dot{\gamma}_0$ is increasing linearly with v_{ram} and quadratically with $\phi_{\text{shotsleave}}$. Due to the additional assumptions made for the localization of the velocity gradients, it decreases with the cubic power of ϕ_{tube}.

Several simulation calculations were performed in order to determine more precisely the shear-rate state in this region. The common conditions of the simulation were as follows:

- The main dimensions of the problem are given in figure 1. In order to estimate the influence of the geometry on the shear rate state, different tube diameters, ϕ_{tube}, were tested (see section 2.1).
- Quadrilateral elements were used to enmesh the geometry. The final mesh was rather coarse at the top of the shot-sleave (averaged element size $\approx 8 \times 8\,\text{mm}^2$) and finer for the rest of the geometry (averaged element size $\approx 1 \times 1\,\text{mm}^2$).

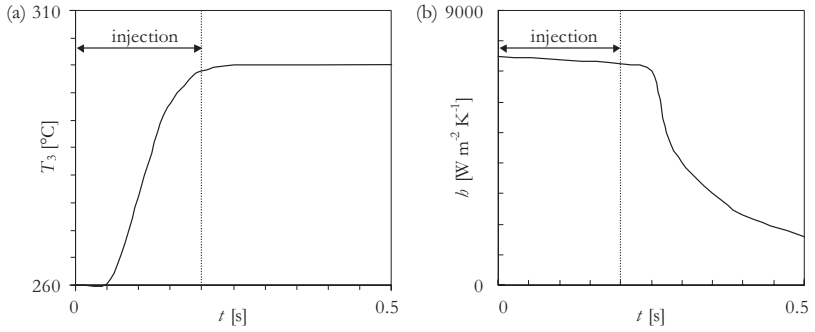

Figure 6. Heating curve, $T_3(t)$, measured during the shaft experiment near the end of the parabolic shape of the shaft (see figure 1(*b*)) (*a*) and heat transfer coefficient, h, between the SSM and the mould calculated by inverse modelling at the same location (*b*). $v_{\text{ram},0} = 0.8\,\text{m s}^{-1}$, $f_{\text{s,ini}} = 0.58$, $\phi_{\text{tube}} = 25\,\text{mm}$ and $\phi_{\text{shaft}} = 18\,\text{mm}$.

- In order to reduce the computation time, only the shot-sleeve and the tube were modelled. At the entrance of the shot-sleeve, the velocity $v_{\text{ram},0}$ was imposed, whereas the atmospheric pressure was applied at the end of the tube.
- The cut-off value $\dot{\gamma}_0$, was taken as the maximum shear rate calculated on the axis under steady-state conditions in the region connecting the shot-sleeve to the tube.
- Adiabatic simulation was performed and the material was assumed to be purely Newtonian, i.e. $\mu = \text{const}$. A first preliminary study showed that the strain-rate state in the shot-sleeve-tube region was independent on the value of μ, at least in the range 10^{-2}–$10^{6}\,\text{Pa s}$. An *a posteriori* study also showed that the recorded cut-off values were not very different from the cut-off values calculated with the temperature-dependent PLCO model. This is essentially due to the fact that this shear rate is mainly dictated by the mass balance and the imposed velocity of the shot-sleeve.

As could be expected from the simple assumptions made previously, the calculated dependence of $\dot{\gamma}_0$ on $v_{\text{ram},0}$ and ϕ_{tube} is very similar to that simply deduced in equation (11):

$$\dot{\gamma}_0 = \chi \left(\frac{\phi_{\text{shotsleave}}}{\phi_{\text{tube}}} \right)^{\beta} \frac{v_{\text{ram},0}}{\phi_{\text{tube}}} \tag{12}$$

The simulation calculations led to $\chi = 2.314$ and $\beta = 2.14$.

4.3. Determination of the consistency value

The parameter B appearing in equation (9*a*) was determined based on the pressures and temperatures measured in the shaft experiments (see figure 1(*b*) for the geometrical configuration and exact positioning of the sensors/thermocouples). More specifically, three different experiments were used, all being performed with $f_{\text{s,ini}} = 0.58$, $\phi_{\text{tube}} = 25\,\text{mm}$, $\phi_{\text{shaft}} = 18\,\text{mm}$, and with a piston velocity $v_{\text{ram},0} = 0.2$, 0.4 and $0.8\,\text{m s}^{-1}$. The pressure recorded at the tube entrance, p_2, (see figure 3) as well as the temperature, T_3, measured in the mould near the end of the parabolic tip of the shaft (see figure 6(*a*)) were used in the numerical simulation as follows:

- Only the tube and shaft geometry was modelled. An imposed velocity v_{tube} $(=v_{\text{ram}}\phi_{\text{ram}}^2/\phi_{\text{tube}}^2)$ was applied at the entrance of the tube, whereas an atmospheric pressure boundary condition was imposed at the exit of the tube.

- Very fine quadrilateral elements were used to enmesh the geometry, so that whatever the axis position, more than ten nodes were present in the radial direction to represent well the boundary layer at the shaft position.
- The initial SSM temperature at the tube entrance was fixed to a constant value corresponding to $f_{s,ini} = 0.58$ (see figure 4(a)). At the end of the tube, an adiabatic boundary condition was imposed.
- The heat transfer coefficient h between the SSM and the tube and between the SSM and the shaft was assumed to be temperature-dependent, but spatially uniform. It was estimated from the temperature T_3 measured in the mould (see figures 1(b) and 6(a)) using inverse modelling [1, 30, 31]. The calculated time-evolution of h for the particular case $v_{ram,0} = 0.8\,m\,s^{-1}$ is also shown in figure 6(b). As can be seen, h is very high (close to $8000\,W\,m^{-2}\,K^{-1}$ for this experiment) during the short injection time; the flowing SSM contacts and quickly heats up the mould from its initial temperature (260°C) to a stationary value of 300°C. At the end of injection (≈0.2 s), the mould temperature remains approximately constant and the heat transfer coefficient h quickly decreases by nearly one order of magnitude ($h \approx 800\,W\,m^{-2}\,K^{-1}$).

4.3.1. Preliminary remarks. Figure 7 shows the flow of the SSM near the shaft tip during an injection performed at $v_{ram,0} = 0.8\,m\,s^{-1}$. The other parameters are: $f_{s,ini} = 0.58$, $\phi_{tube} = 25$ mm and $\phi_{shaft} = 18$ mm. At four different times of injection, the equivalent shear rate $\dot{\gamma}$, and temperature, T, are displayed with different grey levels in the lower, respectively upper, part of the picture. The grey level scale for both fields is linear with maximum and minimum values indicated in the figure caption. As can be seen, the shear rates in the SSM are not zero, even if a free-slip boundary condition was imposed at the SSM-mould interface. This is due to both the geometrical shape of the problem and the temperature field which induces strong gradients in the viscosity, μ. Please note that the equivalent shear rate is maximum at the tip of the shaft where the deflection of the velocity field is maximum (i.e. maximum geometry effect), even though the local temperature is slightly higher. Not only the axisymmetric nature of the problem promotes cooling from the external mould (where the temperature is also slightly lower), but mechanical dissipation (Q_{mech}) is highest in the highly sheared regions near the shaft tip. Although the temperature difference across the SSM region might seem fairly small (<1°C), it must be pointed out that the highest temperature at the shaft tip (569.15°C) corresponds to the nominal temperature of the SSM and the beginning of eutectic solidification (see figure 4(a)), whereas the coldest parts near the tube wall (568.4°C) have about 25% of solidified eutectic (i.e. most of the cooling from the mould is used to solidify isothermally the eutectic). Such a temperature difference induces a solid fraction difference $\Delta f_s \approx 0.16$, which in turns induces a huge variation in μ_0 ($\Delta\mu_0 \approx 1.1 \times 10^4$ Pa s, with $B = 22$, see figure 4(b)). Therefore, even though the total injection time for the SSM to cross the entire small tube is short (<0.05 s), thermal effects are shown to play a key role in the rheological behaviour of the SSM and an adiabatic simulation would be unrealistic.

The non-zero shear rates observed in figure 7 induce a pressure increase ahead of the shaft, as can be seen in figure 8, where the time-evolution of the pressure, p_2, (see figure 1(b) for location) is represented for various boundary conditions, values of the coefficient B (equation (9a)) and velocity of the piston, $v_{ram,0}$:

(a) Comparing for example curve (a) of figure 8 with the experimental curve of figure 3(a), it can be seen that the horizontal plateau at $p = p_{steady}$ is fairly well reproduced by the PLCO model, even though the steady-state calculated pressure of 35 bar is half the value measured in figure 3(a). On the other hand, the short peaks p_{peak} recorded during the shaft experiments

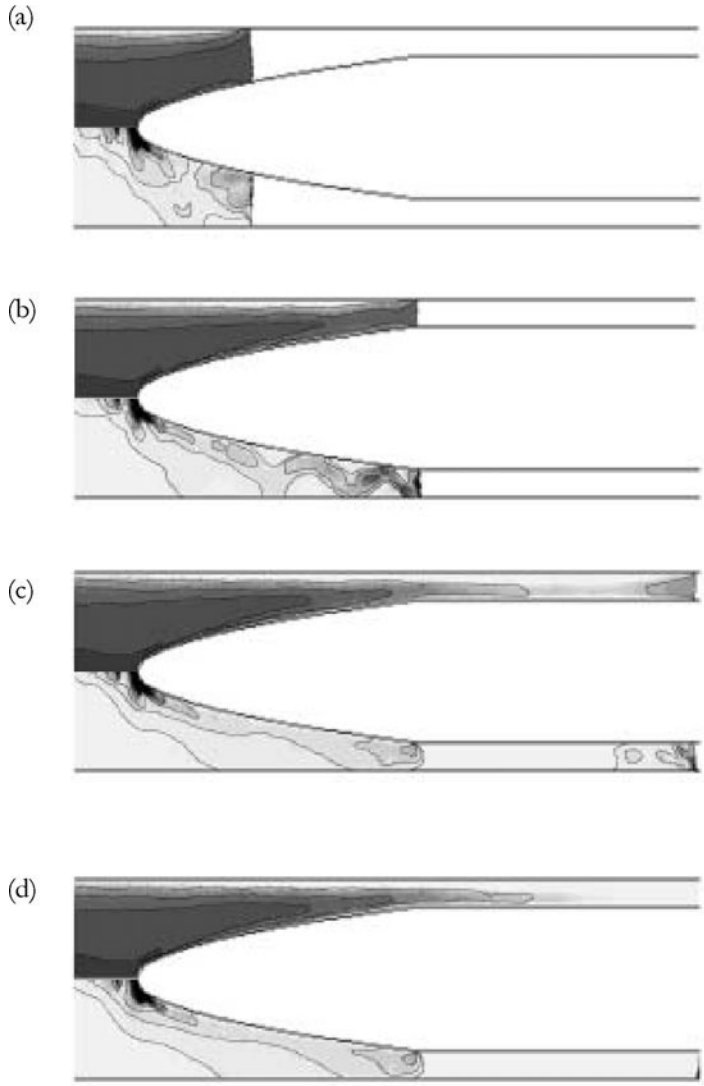

Figure 7. Temperature field (above the shaft) and equivalent shear-rate map (below the shaft) as calculated with the PLCO model implemented in ProCAST^{TM} during the shaft experiment performed at: $v_{ram,0} = 0.8\,m\,s^{-1}$, $f_{s,ini} = 0.58$, $\phi_{tube} = 25\,mm$ and $\phi_{shaft} = 18\,mm$. The four figures correspond to various injection times: $t = 0.009\,s$ (*a*), 0.015 s (*b*), 0.018 s (*c*) and 0.049 s (*d*). For the sake of visibility, the radius (vertical) scale has been expanded by a factor 4. The linear grey scale used for the temperature ranges between 568.4°C (white) and 569.15°C (black), whereas that used for the shear rate goes from $0\,s^{-1}$ (white) to $1500\,s^{-1}$ (black).

(see, e.g. figure 3(*a*)) does not at all appear in figure 8. These pressure peaks are believed to be induced by the solidifying-consolidated advancing mushy front which moves towards the shaft without being well pre-sheared at the entrance of the small tube. Once this front meets the shaft, it has to be broken, thus inducing a high overpressure p_{peaks}. The subsequent part of the feeding, with a material well pre-sheared at the entrance of the tube and with a lower volume fraction of solid, produces lower pressure levels p_{steady}. The very simple PLCO model used in this work is not refined enough to catch these short transient regimes. More sophisticated

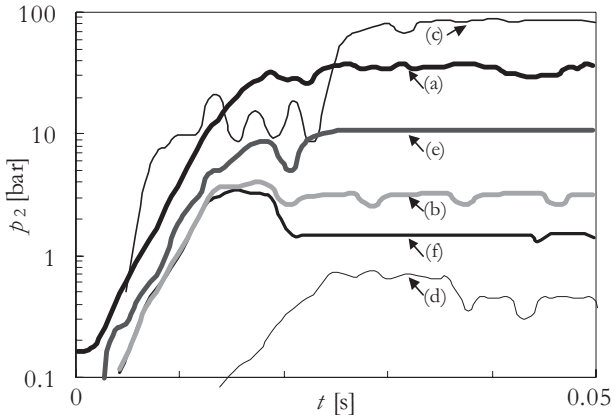

Figure 8. Influence of the heat transfer coefficient, h, ram velocity, $v_{\mathrm{ram},0}$ and constitutive parameter, B, on the evolution of the calculated pressure, p_2, during the shaft experiments performed with $\phi_{\mathrm{tube}} = 25\,\mathrm{mm}$ and $\phi_{\mathrm{shaft}} = 18\,\mathrm{mm}$. The other parameters for each curve are: (a) $v_{\mathrm{ram},0} = 0.8\,\mathrm{m\,s^{-1}}$, h given by figure 6(*b*), $B = 22$; (b) $v_{\mathrm{ram},0} = 0.8\,\mathrm{m\,s^{-1}}$, $h = 0$, $B = 22$; (c) $v_{\mathrm{ram},0} = 0.4\,\mathrm{m\,s^{-1}}$, h given by figure 6(*b*), $B = 22$; (d) $v_{\mathrm{ram},0} = 0.4\,\mathrm{m\,s^{-1}}$, $h = 0$, $B = 22$; (e) $v_{\mathrm{ram},0} = 0.8\,\mathrm{m\,s^{-1}}$, h given by figure 6(*b*), $B = 20$; (f) $v_{\mathrm{ram},0} = 0.8\,\mathrm{m\,s^{-1}}$, h given by figure 6(*b*), $B = 18$.

thixotropic models could account for such complex phenomena, with, in return, an increase of the computation time, since additional internal variables associated with their constitutive equations would be generally required to complete the whole set of involved equations [18–22].

(b) As seen in this figure, some instability occurs in the calculation, especially during the transient regime. These oscillations correspond to the transient time when the flow in the tube reaches the tip of the shaft (i.e. filling of this region), for which the free surface model used to solve equation (5) is certainly not accurate enough. In some way, this corresponds also to the time when a pressure peak is experimentally observed. Once this region is filled, the code then calculates the flow around the shaft (i.e. pseudo-stationary state) and gives much more reliable results. In the subsequent comparisons, only the calculated pressure plateau is compared with the measured value.

4.3.2. Influence of boundary conditions. As can be seen in figure 8, the mechanical and thermal boundary conditions defined for the SSM-mould interface play a crucial role in the numerical results. For the same injection speed ($v_{\mathrm{ram},0} = 0.8\,\mathrm{m\,s^{-1}}$) and parameter B, the replacement of the heat transfer coefficient, h, given by figure 6(*b*) (curve (a)) by an adiabatic condition (curve (b)) drastically decreases the pressure, p_2, by a factor 20. On the other hand, it was shown in section 2.2 that an increase in the recorded pressure p_2 with a decrease in the piston ram, $v_{\mathrm{ram},0}$, could be a consequence of thermal effects. Such an observation is confirmed by the simulation results shown in figure 8, providing the heat transfer between the SSM and the mould is 'turned on'. Comparing curves (a) and (c) in figure 8, it can be seen that a variation of the ram velocity, $v_{\mathrm{ram},0}$, from 0.8 to $0.4\,\mathrm{m\,s^{-1}}$ almost doubles the pressure, p_2, at steady state. Moreover, using purely adiabatic boundary conditions, the other trend is observed (compare curves (b) and (d) for which the same decrease in $v_{\mathrm{ram},0}$ now decreases the pressure p_2 by almost a factor 2).

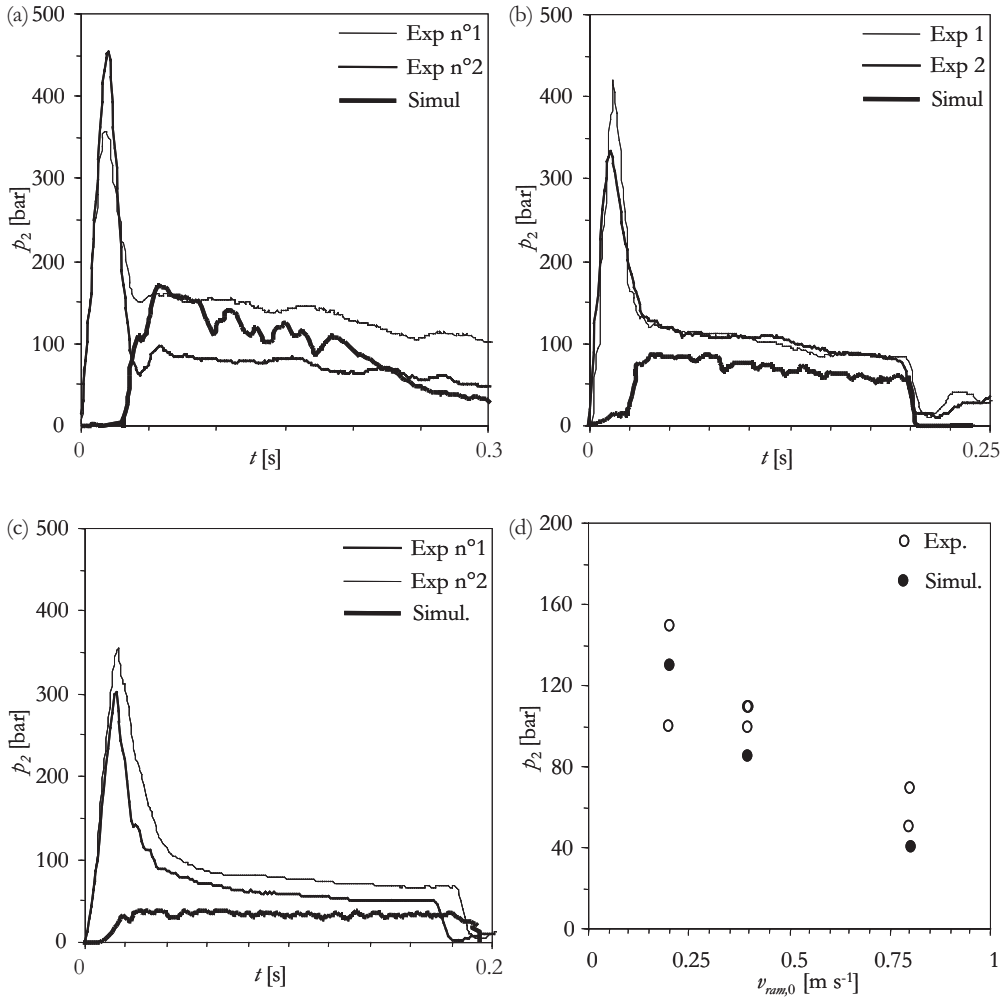

Figure 9. Time-evolution of the measured and simulated pressures, p_2, for $v_{\mathrm{ram},0} = 0.2\,\mathrm{m\,s^{-1}}$ (*a*), $0.4\,\mathrm{m\,s^{-1}}$ (*b*) and $0.8\,\mathrm{m\,s^{-1}}$ (*c*). The measured and computed pressures, p_2, at 'steady-state' are compared as a function of $v_{\mathrm{ram},0}$ in (*d*).

4.3.3. Results. The goal of the shaft experiment simulation is to ultimately determine the missing constitutive parameter B appearing in equation (9*a*). All other conditions remaining the same, the dependence of the calculated pressure, p_2, on this parameter is shown in figure 8 (compare curves (a), (e) and (f)). When B is decreased from 22 to 18, the pressure, p_2, is decreased by one order of magnitude (from 35 to 1.5 bar). Increasing this value beyond 22 could have allowed to match the calculated steady state pressure, p_{steady}, with the value measured for $v_{\mathrm{ram},0} = 0.8\,\mathrm{m\,s^{-1}}$ (see figure 3(*b*) where $p_{\mathrm{steady}} = 70\,\mathrm{bar}$). However, when considering all the initial piston velocities (0.2, 0.4 and $0.8\,\mathrm{m\,s^{-1}}$), it was found that $B = 22$ could best reproduce the six experiments. The simulated results are compared with the experiments in figures 9(*a*)–(*c*) for $v_{\mathrm{ram},0} = 0.2\,\mathrm{m\,s^{-1}}$, $0.4\,\mathrm{m\,s^{-1}}$ and $0.8\,\mathrm{m\,s^{-1}}$, respectively. In each figure, the pressure evolution for the two experiments are clearly identified by the presence of a peak, whereas the simulation performed with $B = 22$ does not. These results are summarized in

figure 9(*d*), where the simulated 'steady-state' pressure is compared with the experimental result as a function of the piston ram velocity. Considering both the large scattering of the experimental points and the strong assumptions made for the simulation, the agreement is satisfactory and more important, the trend is well reproduced (decrease of p_{steady} with increasing $v_{\text{ram},0}$).

5. Validation

In the previous section, two constitutive parameters of the PLCO model (equations (6), (8) and (9)) were determined on the basis of the pressures and temperatures measured during the shaft experiments: the cut-off value, $\dot{\gamma}_0$ (equation (12)), and the value of B (equation (9*a*)). The values of all the PLCO model parameters are summarized in table 1. In this section, this PLCO model is now used to simulate the filling of the reservoir in the Poiseuille-type experiments (see figure 1(*a*)) and to check whether this model is capable of reproducing the various filling behaviours observed when varying in particular the initial volume fraction of solid, $f_{\text{s,ini}}$ [10]. Fixing ϕ_{tube} and $v_{\text{ram},0}$ to 25 mm and 0.8 m s^{-1}, respectively, three simulations were performed under the following conditions:

- Only the long tube and the reservoir were modelled in order to reduce the computation time. A $v_{\text{tube}}(v_{\text{ram}}(t))$ boundary condition was applied at the entrance of the tube.
- Fine quadrilateral elements were used to enmesh the geometry (averaged mesh size $\approx 1.5 \times 1.5\,\text{mm}^2$).
- For the three experiments, the temperature at the tube entrance was fixed to a constant value corresponding to $f_{\text{s,ini}} = 0.73$, 0.58 and 0.52 (see figure 4(*a*)).
- The temperature of the mould (i.e. tube and reservoir) and the heat transfer coefficient between the SSM and the mould were set constant and equal to 250°C and 500 W m^{-2} K^{-1}, respectively. The last value was lowered as compared with that found in the shaft experiments because of the much lower pressure level.
- The end of each experiment was supposed to be reached after 1 s, corresponding to a stop of the SSM deformation in the reservoir.

Taking advantage of the axisymmetric nature of the problem, figure 10 shows the evolutions during filling of the equivalent shear-rate, $\dot{\gamma}$, and of the viscosity, μ, in the upper, respectively lower, part of the reservoir. The simulation corresponds to an initial volume fraction of solid, $f_{\text{s,ini}} = 0.58$. In this example, the SSM solidified in the reservoir after the injection was interrupted had the shape of a 'disk + shell' [10]. The grey level scales used for both the shear-rate and viscosity fields are linear (the minimum and maximum values are indicated in the figure caption). The six figures shown in figure 10 correspond to various injection times, between 0.075 and 1 s.

Several remarks can be made. First, for $0 < t < 0.1$ s, the velocity of the piston was constant (i.e. $v_{\text{ram}}(t) = v_{\text{ram},0}$) and so was the velocity of the SSM in the tube. As can be seen in figures 10(*a*) and (*b*), the SSM cross-section at the entrance of the reservoir remains approximately constant and equal to ϕ_{tube}. The shear rate is zero in the tube (free-slip, no shaft) and very high at the contact with the bottom of the reservoir. The increase of the viscosity, μ, at the periphery of the SSM in contact with the mould (tube or reservoir) is mainly due to a temperature decrease induced by the imposed thermal boundary condition at this interface.

Second, for $0.1\,\text{s} < t < 0.15\,\text{s}$, the velocity of the piston, $v_{\text{ram}}(t)$, was rapidly decreased: this can be noticed by a reduction of the SSM cross-section entering the reservoir (figure 10(*c*)). Third, for $0.15\,\text{s} < t < 0.2\,\text{s}$, the SSM is still flowing in the reservoir, even though $v_{\text{ram}}(t)$ is close to zero, as a result of inertia effects (first two terms in equation (2)). However, as the

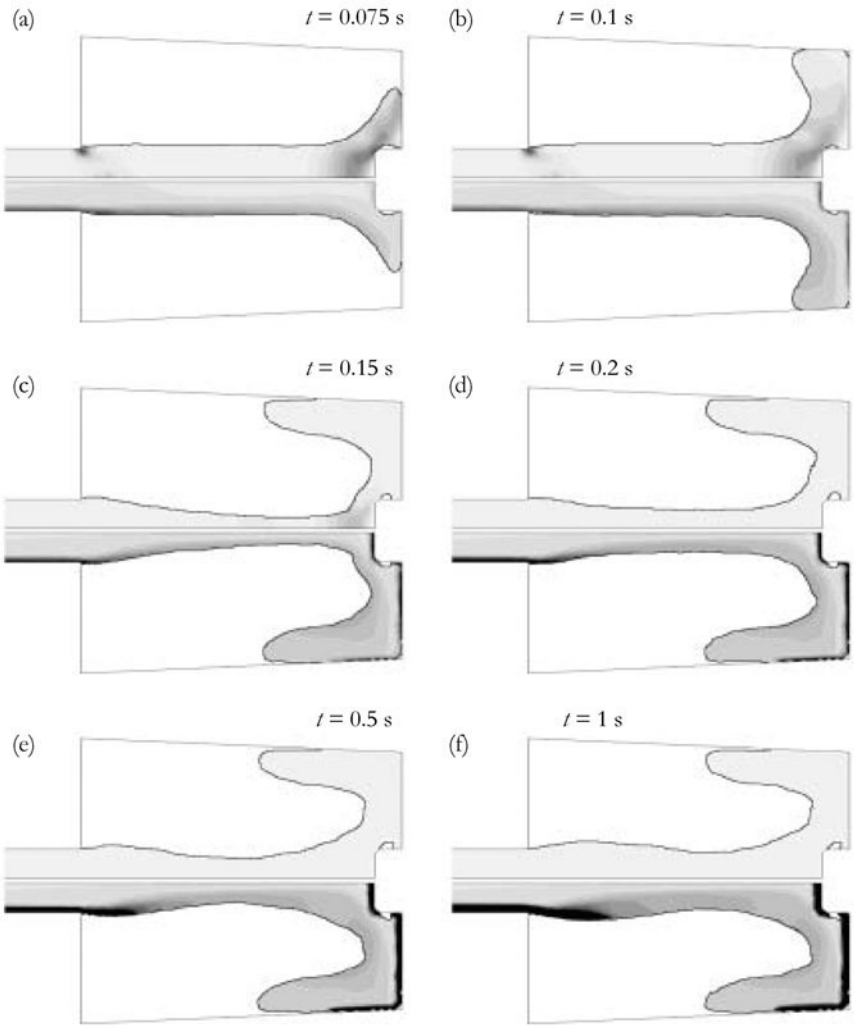

Figure 10. Simulation of the reservoir filling during the Poiseuille-type experiment performed at $v_{\mathrm{ram},0} = 0.8\,\mathrm{m\,s^{-1}}$, $\phi_{\mathrm{tube}} = 25\,\mathrm{mm}$ and $f_{\mathrm{s,ini}} = 0.58$, at six different times. In each figure, the equivalent shear rate and the SSM viscosity are displayed in the upper, respectively lower, part of the reservoir with various grey levels. The grey scales are linear and spread from $0\,\mathrm{s^{-1}}$ (white) to $3000\,\mathrm{s^{-1}}$ (black) for the equivalent shear rate, and from 0 Pa s (white) to 150 Pa s (black) for the viscosity.

SSM part in contact with the end of the reservoir has further solidified and thickened, it does not move any more during this time interval. Consequently, the section of the inner part of the SSM becomes wider (cf figures 9(*c*) and (*d*)). Finally, for $0.2\,\mathrm{s} < t < 0.5\,\mathrm{s}$, inertia effects vanish and further solidification of the SSM increases its viscosity. Since the SSM has nearly stop to move, the equivalent shear rate is reduced almost to zero.

The experimental axial sections of the reservoir fillings obtained for different initial solid fractions are compared with numerical simulation in figure 11. For each initial solid fraction, the shape of the SSM that has solidified at the surface of the reservoir when the experiment was interrupted is displayed in the lower part, whereas the simulated one is shown in the upper one. As shown in this figure, all the experimental axial sections were qualitatively

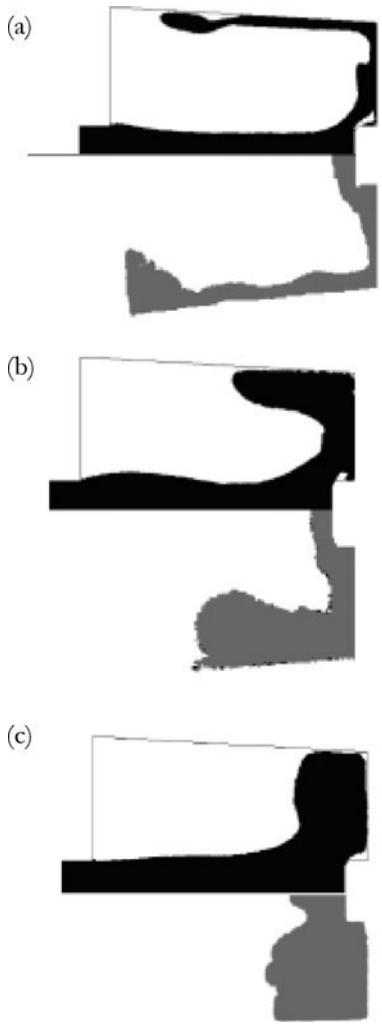

Figure 11. Comparison between experimental and simulated reservoir fillings when $v_{\mathrm{ram},0} = 0.8\,\mathrm{m\,s^{-1}}$, $\phi_{\mathrm{tube}} = 25\,\mathrm{mm}$ and for $f_{\mathrm{s,ini}} = 0.52$ (*a*), 0.58 (*b*) and 0.73 (*c*). In each figure, the simulated and the experimental filling are displayed in the upper, respectively lower, part of the reservoir.

well reproduced by the simulation: 'disk' filling is obtained for high initial solid fraction ($f_{\mathrm{s,ini}} = 0.73$, figure 11(*c*)), a 'disk + shell' forms when $f_{\mathrm{s,ini}} = 0.58$ (figures 11(*b*) and 10), whereas a thin 'shell' follows the surface of the reservoir at the lowest initial solid fraction ($f_{\mathrm{s,ini}} = 0.52$, figure 11(*a*)). Please note the drastic change in the reservoir filling morphology when $f_{\mathrm{s,ini}}$ is only varied from 0.58 to 0.52!

6. Discussion and conclusion

The aim of this work was to model the industrial thixocasting process using a PLCO model implemented in a commercial numerical software. A first part consisted in performing Poiseuille-type experiments, with or without a parabolic shaft inserted in the tube. During these experiments, different process parameters were varied in order to determine the constitutive

parameters of the PLCO model. To reach such a goal, strong assumptions were made, both on the constitutive parameters and on the boundary conditions. As a matter of fact, most of the parameters of the PLCO model were given by previously published data and only the shear cut-off value, $\dot{\gamma}_0$, and the parameter, B, of equation (9a) were determined by the simulation. The cut-off value is an extrinsic parameter depending mainly on the geometry and mechanical boundary conditions. The intrinsic parameter B dictates the solid fraction-dependence of the viscosity. Since the thermal boundary condition between the SSM and the mould cannot be considered as adiabatic, the value of this parameter was shown to have a strong influence on the mould filling simulation. Based on the shaft experiment simulations, a B-value of 22 seemed to best reproduce the steady-state pressure measured ahead of the shaft. Using the values summarized in table 1, the PLCO model was then capable of reproducing fairly accurately the shape of the SSM part that had solidified in the reservoir during interrupted injection experiments.

These results are encouraging, even though they are still semi-quantitative. In particular, the importance of the thermal effects on the SSM flow was clearly evidenced for the industrial process, even with a short injection time (<1 s). This issue has been rarely addressed in laboratory-scale experiments, which have essentially focused on the shear-rate (and time) dependence of the viscosity under isothermal conditions. Likewise, the use of the PLCO model is very simple, since only six rheological parameters are involved. However, these result should still be viewed as preliminary since many hypotheses have been made in the simulation (e.g. free-slip, uniform heat transfer coefficient). In order to give more quantitative results, several limitations of this methodology should be removed:

(a) The Poiseuille-type experiments, with or without shaft, were performed on a production-scale injection machine and are thus very close to industrial thixocasting conditions. Hence, from an industrial point of view, they brought a valuable understanding of the process: the injection process cannot be considered as isothermal, deformation is fast and heterogeneous. However, from a modelling point of view, such a complex loading mixes also the various aspects of the problem. For instance, a perfect knowledge of the mechanical boundary condition is required if an accurate knowledge of the rheological behaviour is to be obtained. Such is not the case in this work. From a mechanical point of view, free-slip was assumed at the SSM-mould interface, owing to the presence of a thin liquid of eutectic composition (figure 2(b)). Although it appears realistic to consider this liquid layer as a perfect lubricant (and not model it), it would be more realistic to introduce a boundary layer approach in the simulation in a way similar to aerodynamics calculations. From a thermal point of view, the heat transfer coefficient between the mould and the SSM is certainly not a unique function of time (figure 6): it also depends on the position, local pressure, volume fraction of solid, etc. As this study clearly revealed the importance of the thermal exchanges during mould filling, heat transfer between the SSM and the mould should be further investigated using inverse modelling.

(b) In future investigations, the mechanical boundary conditions and rheological behaviour of the SSM should be investigated separately, but under conditions close to the industrial process. Laboratory-scale isothermal investigations of the SSM behaviour performed under no-slip condition are certainly very valuable, but they should be extended to the very high shear rates encountered in the industrial process (typically $10^3\ \mathrm{s}^{-1}$). Using then a well-defined rheological law for the SSM, instrumented experiments combined with numerical simulation will allow to determine more accurately the boundary conditions prevailing in the industrial process.

(c) SSM are thixotropic materials, i.e. their structure can evolve during loading. The introduction of a cut-off value in the power-law model is a first, and very simple attempt to

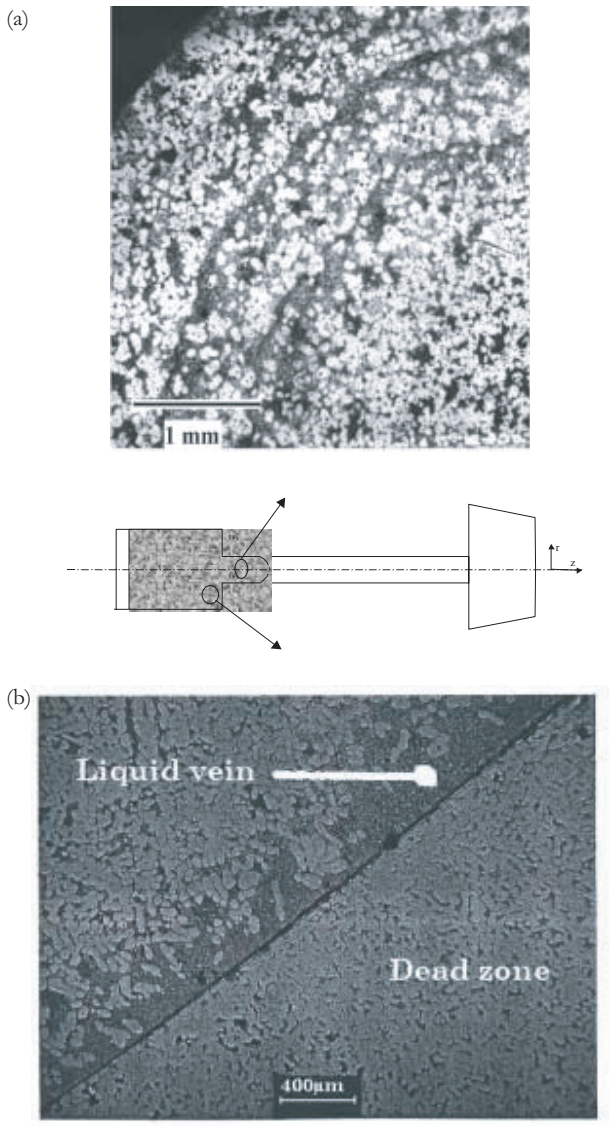

Figure 12. Cross-section (*a*) of the SSM cylinder solidified in the tube of a Poiseuille-type experiment. The eutectic-rich concentric rings are due to veins of liquid formed in the shot-sleeve. Such a vein formed at the limit of the dead zone of the shot-sleeve is shown in the longitudinal section (*b*).

account for these structural evolutions. However, the cut-off values defined in ProCAST^{TM} are fixed before the simulation starts. The cut-off value should be position-dependent and linked to a fluid particle, i.e. the viscosity history should be followed along streamlines.

(d) During deformation, mechanically induced phase separation has been clearly evidenced in SSM processing. This has been shown for the peripheral zone located near the external surface of the tube (figure 2(*b*)). Highly-rich eutectic regions has also been observed in the form of internal and concentric rings in the tube (see figure 12(*a*)). These rings

could be correlated to veins of liquid formed early in the shot-sleeve (see figure 12(*b*)). These veins result from mechanical instabilities generated in a solid skeleton which is not uniformly sheared. In figure 12(*b*), the vein of eutectic liquid at 45° was shown to be due to the 'dead' zone at the bottom right corner of the shot-sleeve, i.e. a zone which is almost not sheared and only compressed. The compression of the dead zone induces a 'sponge-like' effect, i.e. the intergranular liquid is expulsed of the zone and flows in the vein. Please note that the volume fraction of primary aluminum phase is much higher in this zone. Obviously, such a complex behaviour cannot be predicted with a one-phase model. Two-phases models could possibly address this issue, providing damage mechanisms and solid skeleton break-up criteria will be included in such approaches, which is not yet the case.

Acknowledgments

The authors would like to thank Alusuisse (now Alcan) Technology Management, Neuhausen-am-Rheinfall, and the Commission pour la Technologie et l'Innovation, Bern, Switzerland, for their financial support within the framework of the projects CTI 2942.1 and 3753.1.

References

[1] Paradies C, Rappaz M, Imwinkelried T and Gabathuler J-P 1997 *Proc. EPD Congress* ed Mishra, p 725
[2] Flemmings M C 1991 Behavior of metal alloys in the semi-solid state *Metall. Trans.* B **22** 269–93
[3] Martin C L, Kumar P and Brown S 1994 Constitutive modelling and characterization of the flow behavior of semi-solid metal alloy slurries—II. Structural evolution under shear deformation *Acta Metall. Mater.* **42** 3603–14
[4] Salvo L, Loué W and Suéry M 1995 Influence of prior solidifications on the structure and rheological behavior of partially remelted Al–Si alloy *ISIJ Int.* **35** 798–804
[5] Loué W 1992 Evolution microstructurale et comportement rhéologique d'alliage Al–Si à l'état semi-solide *PhD Thesis* Institut National Polytechnique de Grenoble, Grenoble, France
[6] Liechti T, Chen Z W, Davidson C J and Dahle A K 1998 Casting defects and tensile properties of semi-solid cast AZ91 *Proc. 5th Int. Conf. on SS Processing of Alloys and Composites* ed A Kumar Bashin *et al* (USA: Colorado School of Mines) pp 505–12
[7] Cho W G and Kang CG 2000 Mechanical properties and their microstructure evaluation in the thixoforming process of semi-solid aluminium alloys *J. Mater. Process. Technol.* **105** 269–77
[8] Gabathuler J-P, Barra D, Krähenbühl Y and Weber J C 1990 *Proc. 2nd Int. Conf. on SS Processing of Alloys and Composites* (Cambridge, MA, USA: MIT Press) p 119
[9] Koke J, Hufschmidt M, Modigell M, Heine C, Han S, Stapf S and Petera J 2000 Segregation and wall slip in semi-solid alloys: measurement, modelling and simulation *Proc. 6th Int. Conf. on SS Processing of Alloys and Composites* ed G L Chiarmetta and M Rosso (Italy: Edimet) pp 623–8
[10] Paradies C, Rappaz M, Imwinkelried T and Gabathuler J-P 1998 Modeling the rheology of semi-solid metal alloys during die casting *Proc. ICMCWASP (San Diego, USA)* p 933
[11] Nguyen T Y, Favier D and Suéry M 1994 Theoretical and experimental study of the isothermal behavior of alloys in the semi-solid state *Int. J. Plasticity* **10** 663–93
[12] Gebelin J-C, Favier D, Suéry M and Guarnéri C 1996 A FEM simulation of semi-solid material behavior *Proc. 4th Int. Conf. on SS Processing of Alloys and Composites* ed D H Kirkwood and P Kapranos (UK: University of Sheffield) pp 126–31
[13] Martin C L, Favier D and Suéry M 1997 Viscoplastic behaviour of porous metallic materials saturated with liquid—Part I. Constitutive equations—Part II. Experimental identification on a Sn–Pb alloy *Int. J. Plasticity* **13** 237–59
[14] Burgos G R, Alexandrou A N and Entov V 1998 Two-phase flow of semi-solid materials *Proc. 5th Int. Conf. on SS Processing of Alloys and Composites* ed A Kumar Bashin *et al* (USA: Colorado School of Mines) pp 217–24
[15] Modigell M, Koke J and Petera J 1998 Two-phase model for metal alloys in the semi-solid state *Proc. 5th Int. Conf. on SS Processing of Alloys and Composites* ed A Kumar Bashin *et al* (USA: Colorado School of Mines) pp 317–26

[16] Kang C G, Jung H K and Jung K W 1999 Finite Element analysis with deformation behavior modelling of globular microstructure in forming process of semi-solid materials *J. Mater. Process. Technol.* **41** 1423–45
[17] Ko D-C, Min G-S, Kim B-M and Choi J-C 2000 Finite Element analysis for the semi-solid state forming of aluminium alloy considering induction heating *J. Mater. Process. Technol.* **100** 95–104
[18] Kumar P, Martin C L and Brown S 1994 Constitutive modelling and characterization of the flow behavior of semi-solid metal alloy slurries—I. The flow response *Acta Metall. Mater.* **42** 3595–602
[19] Quaak C J, Katgerman L and Kool W H 1996 Viscosity evolution of partially solidified aluminium slurries after a shear rate jump *Proc. 4th Int. Conf. on SS Processing of Alloys and Composites* ed D H Kirkwood and P Kapranos (UK: University of Sheffield) pp 35–9
[20] Alexandrou A N, Burgos G R and Entov V 1999 Mathematical and computational modelling of die filling in semi-solid metal processing *J. Mater. Process. Technol.* **96** 59–72
[21] Wahlen A 2000 Modeling the thixotropic flow behavior of semi-solid aluminium alloys *Proc. 6th Int. Conf. on SS Processing of Alloys and Composites* ed G L Chiarmetta and M Rosso (Italy: Edimet) pp 565–70
[22] Modigell M and Koke J 2001 Rheological modelling on semi-solid metal alloys and simulation of thixocasting processes *J. Mater. Process. Technol.* **111** 53–8
[23] Bowen R M 1976 *Continuous Physics. III, Mixture and EM Field Theories* (New York, USA: Academic)
[24] Gebelin J-C, Geindreau C, Orgéas L, Royer P, Favier D and Auriault J-L 2000 Influence of liquid flow through the solid skeleton on the overall deformation of metallic alloys in semi-solid state *Proc. 6th Int. Conf. on SS Processing of Alloys and Composites* ed G L Chiarmetta and M Rosso (Italy: Edimet) pp 155–60
[25] Cheng D C and Evans F 1965 Phenomenological characterization of the rheological behavior of inelastic reversible thixotropic and antithixotropic fluids *Br. J. Appl. Phys.* **16** 1599–617
[26] Laxmanan V and Flemmings M C 1980 Deformation of a semi-solid Sn15%Pb alloy *Metall. Trans.* A **11** 1927–37
[27] Suéry M and Flemmings M C 1982 Effect of strain rate on deformation behavior on semi-solid dendritic alloys *Metall. Trans.* A **13** 1809–19
[28] 1995 *ProCast*^{TM} *User Manual* version 3.0, UES Inc
[29] Nguyen T Y 1991 Modélisation du comportement rhéologique d'alliages à l'état semi-solide *PhD Thesis* Institut National Polytechnique de Grenoble, Grenoble, France
[30] Rappaz M, Desbiolles J-L, Drezet J-M, Gandin C-A, Jacot A and Thévoz P 1995 *Proc. ICMCWASP VII* ed M Cross and J Campbell (USA: Warrendale) p 449
[31] Rappaz M, Bellet M and Deville M 2003 *Modeling in Materials Science and Engineering* (Berlin: Springer) p 447